Stem Cell Reports
Report
ISSCR
OPEN ACCESS

Relative Levels of *Gli1* and *Gli2* Determine the Response of Ventral Neural Stem Cells to Demyelination

Daniel Z. Radecki,[1] Heather M. Messling,[1] James R. Haggerty-Skeans,[2] Sai Krishna Bhamidipati,[1] Elizabeth D. Clawson,[1] Christian A. Overman,[1] Madison M. Thatcher,[1] James L. Salzer,[2,3] and Jayshree Samanta[1,3,*]

[1]Stem Cell and Regenerative Medicine Center, Department of Comparative Biosciences, School of Veterinary Medicine, University of Wisconsin-Madison, Madison, WI 53706, USA
[2]Department of Neuroscience and Physiology, Neuroscience Institute, NYU Langone Medical Center, New York, NY 10016, USA
[3]Co-senior author
*Correspondence: jayshree.samanta@wisc.edu
https://doi.org/10.1016/j.stemcr.2020.10.003

SUMMARY

Enhancing repair of myelin is an important therapeutic goal in many neurological disorders characterized by demyelination. In the healthy adult brain, ventral neural stem cells (vNSCs) in the subventricular zone, marked by GLI1 expression, do not generate oligodendrocytes. However, in response to demyelination, their progeny are recruited to lesions where they differentiate into oligodendrocytes and ablation of GLI1 further enhances remyelination. GLI1 and GLI2 are closely related transcriptional activators but the role of GLI2 in remyelination by vNSCs is not clear. Here, we show that genetic ablation of *Gli1* in vNSCs increases GLI2 expression and combined loss of both transcription factors decreases the recruitment and differentiation of their progeny in demyelinated lesions. These results indicate that GLI1 and GLI2 have distinct, non-redundant functions in vNSCs and their relative levels play an essential role in the response to demyelination.

INTRODUCTION

Neural stem cells in the subventricular zone (SVZ) of adult mammalian brains are a heterogeneous population (Chaker et al., 2016), which include cells expressing GLI1 residing in the ventral SVZ (Ahn and Joyner, 2005). These ventral neural stem cells (vNSCs) do not generate oligodendrocyte progenitor cells (OPCs) or mature oligodendrocytes (OLs) and their progeny are excluded from all white matter tracts in the adult mouse brain. Instead, the vNSCs generate interneurons and astrocytes in the olfactory bulb (OB) and astrocytes in the gray matter of the adult brain (Garcia et al., 2010; Ihrie et al., 2011). Remarkably, GLI1 vNSCs respond to loss of OLs by recruitment of their progeny and by differentiating into OLs in demyelinating lesions (Samanta et al., 2015; Sanchez and Armstrong, 2018). The number of vNSC-derived cells recruited to the lesions and the proportion of these cells generating remyelinating OLs increases significantly when GLI1 is inactivated genetically or pharmacologically (Samanta et al., 2015).

GLI1 and GLI2 act as major transcriptional activators of the Sonic hedgehog (Shh) pathway, but have different expression patterns in the SVZ (Petrova et al., 2013). While genetic ablation of *Gli1* does not affect development, knocking out either *Gli2* alone (Mo et al., 1997) or both *Gli1* and *Gli2* (Park et al., 2000) is embryonic lethal, indicating their distinct functions. In this study, we found an increase in GLI2 expression in the SVZ of *Gli1* null mice in response to demyelination leading us to examine whether GLI2 plays a role in the enhanced remyelination observed by GLI1 inhibition. Our results show that the combined ablation of *Gli1* and *Gli2* in vNSCs not only impairs the recruitment of their progeny into demyelinated lesions, but also their differentiation into OLs. In addition, the *in vivo* loss of both transcription factors substantially directs the migration of cells derived from vNSCs away from the lesions, thus indicating that the physiological migration of vNSC-derived cells to the OB versus recruitment to lesions are mechanistically distinct. These results highlight the non-overlapping functions of GLI1 and GLI2 in response to a demyelinating injury.

RESULTS

Gli2 Is Upregulated in vNSCs following Demyelination

GLI2 is broadly expressed in the NSCs along the entire adult SVZ (Petrova et al., 2013) in contrast to GLI1, which is limited ventrally in healthy mice. We examined GLI2 expression in the SVZ of *Gli1-LacZ* knockin mice after inducing demyelination with cuprizone, a toxin that causes oligodendroglial cell death (Matsushima and Morell, 2001). We observed a significant (2.3 ± 0.37-fold) increase in the levels of *Gli2* mRNA in the $Gli1^{LacZ/LacZ}$ SVZ lacking GLI1 expression at 6 weeks of cuprizone diet as compared with the SVZ of healthy mice on a regular diet

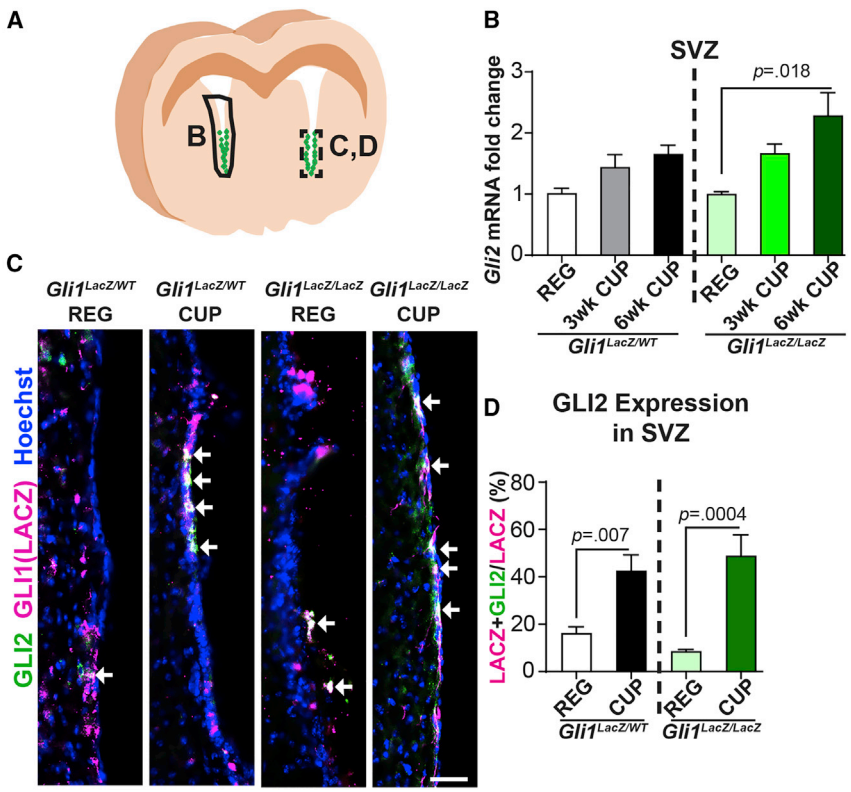

Figure 1. *Gli2* Expression Increases in the *Gli1*^{NULL} SVZ on Demyelination

(A) Schematic for tissue harvested for qRT-PCR in (B) and immunofluorescence in (C and D).

(B) qRT-PCR showing *Gli2* mRNA expression in the SVZ on demyelination induced with 6 weeks of cuprizone diet.

(C) Immunofluorescence for co-localization of Gli2 (green) and LacZ (magenta) in the ventral SVZ of mice on 6 weeks of regular or cuprizone diets. Scale bar, 50 μm. Hoechst, nuclei.

(D) Quantification of the Gli1-LacZ NSCs co-expressing Gli2 in (C).

One-way ANOVAs with Tukey's post-hoc t tests; data presented as mean ± SEM; n = 3 mice/group. SVZ, subventricular zone; CUP, cuprizone diet; REG, regular diet.

(Figures 1A and 1B). More importantly, there was a significant increase in the proportion of GLI1 vNSCs co-expressing GLI2 in both the *Gli1*$^{LacZ/LacZ}$ SVZ (48.9% ± 4.4% on a cuprizone diet versus 8.6% ± 0.7% on a regular diet) and the *Gli1*$^{LacZ/WT}$ SVZ (42.6% ± 6.7% on a cuprizone diet versus 16.3% ± 2.6% on a regular diet) at peak demyelination (Figures 1C and 1D). Thus, *Gli2* is upregulated in the vNSCs in response to demyelination, suggesting a role in remyelination.

Combined Loss of *Gli1* and *Gli2* Decreases the Recruitment of vNSC-Derived Cells to Demyelinated Lesions

To determine if GLI2 expression is required for recruitment of vNSCs-derived cells to the demyelinated lesion, we examined the effects of conditional ablation of *Gli2* specifically in adult GLI1 vNSCs using *Gli1*^{CreER};*Gli2*^{FX} mice. After confirming that *Gli2* is ablated from 84.7% ± 0.4% of the GLI1 vNSCs (Figures S1A and S1B), we analyzed the fate of the GLI1 vNSC progeny in the corpus callosum (CC) at 2 weeks of recovery from a cuprizone diet (Figures 2A and 2B). As expected from previous studies, *Gli1* fate-mapped cells were observed in the CC only upon demyelination and significantly more *Gli1* fate-mapped cells were found in the *Gli1*^{NULL} CC compared with the *Gli1*^{HET} CC when GLI2 expression was intact (Figure 2B) (Samanta et al., 2015). The number of infiltrating *Gli1* fate-mapped cells in *Gli1*^{HET} CC did not change upon ablation of *Gli2* (Figures 2A and 2B). In contrast, loss of one copy of *Gli2* in the *Gli1*^{NULL} mice (*Gli1*^{NULL};*Gli2*^{HET}) reduced the number of *Gli1* fate-mapped cells in the CC by 81.5% ± 5.6%, and complete ablation of *Gli2* (*Gli1*^{NULL};*Gli2*^{NULL}) reduced the number of fate-mapped cells by 88.7% ± 4.3% compared with the *Gli1*^{NULL} mice with intact *Gli2* expression (*Gli1*^{NULL};*Gli2*^{WT}) (Figures 2A and 2B) without altering the extent of demyelination (Figures S2A and S2B). Thus, haploinsufficiency of *Gli2* in the *Gli1*^{NULL} vNSCs is sufficient to reverse the enhanced recruitment of their progeny into the CC upon demyelination.

Although loss of *Gli2* does not alter neurogenesis from vNSCs in the healthy SVZ (Petrova et al., 2013), its role in maintaining neurogenesis along with quiescence and activation of these cells upon demyelination is unknown. We quantified the *Gli1* fate-mapped cells in the SVZ that co-express NESTIN, a marker of activated NSCs and GFAP, a marker of quiescent NSCs at peak demyelination (Codega et al., 2014). Loss of one or both copies of *Gli2* did not change the number of *Gli1* fate-mapped cells co-expressing NESTIN at peak demyelination or GFAP at 2 weeks of recovery from demyelination in the *Gli1*^{HET} or *Gli1*^{NULL} SVZ (Figures 2C–2E). To further examine the effect of *Gli2* on proliferation of *Gli1* fate-mapped vNSCs from adult *Gli1*^{HET} and

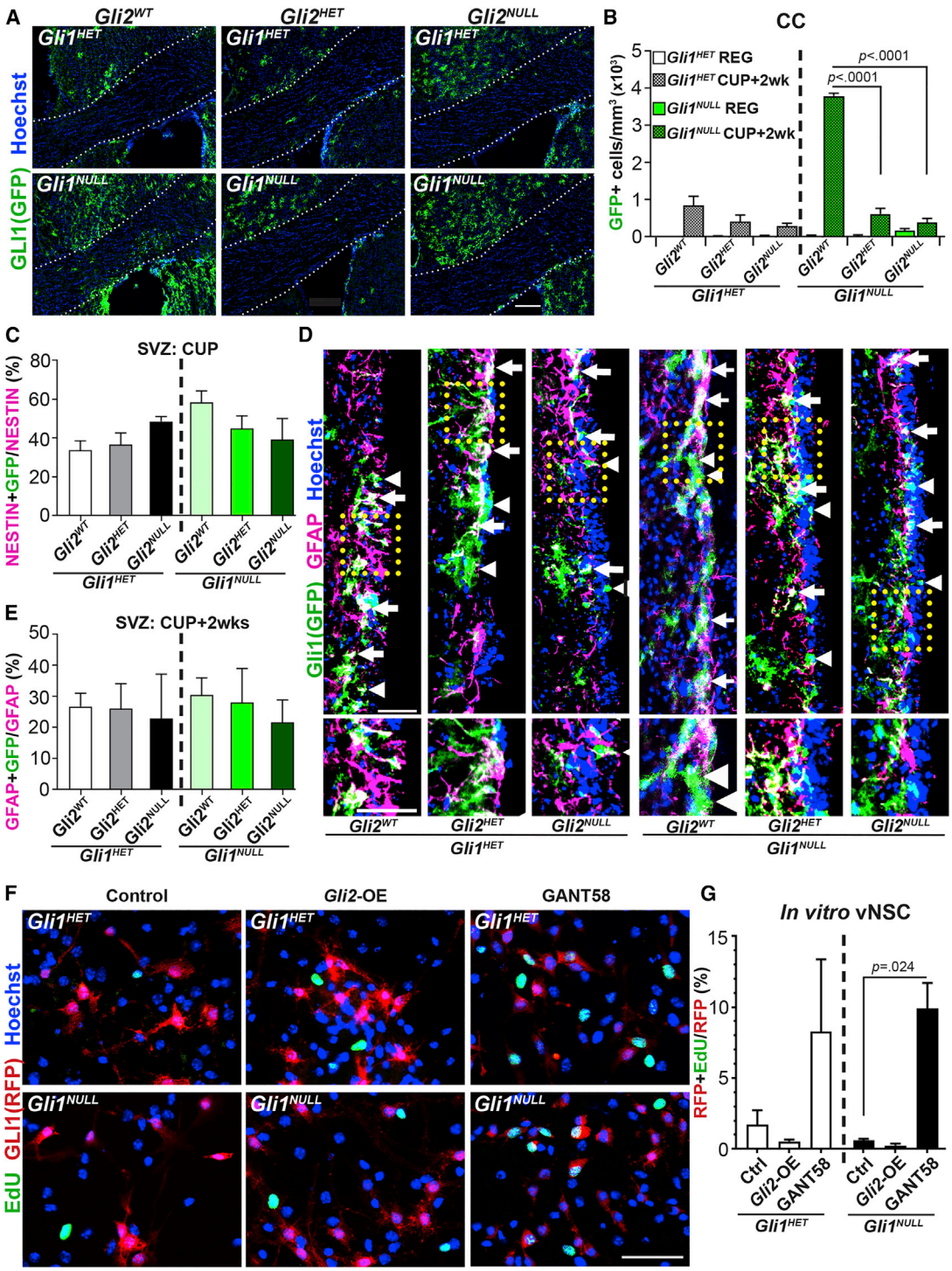

Figure 2. Ablation of *Gli2* Decreases Recruitment of *Gli1*^{NULL} vNSC Progeny to the White Matter Lesion.

(A) Immunofluorescence for GFP + fate-mapped Gli1 cells in the CC of mice at 2 weeks of recovery from a cuprizone diet. Scale bar, 200 μm, n = 5 mice/group.

(B) Quantification of the total number of fate-mapped *Gli1*^{HET} (white) and *Gli1*^{NULL} (green) vNSCs in (A). Two-way ANOVAs with Tukey's post-hoc t tests within *Gli1*^{HET} and *Gli1*^{NULL} groups; mean ± SEM. n = 5 mice/genotype.

(C) Quantification of the proportion of GFP + fate-mapped *Gli1* vNSCs co-expressing Nestin in the SVZ at 6 weeks of cuprizone diet. n = 3 mice/genotype.

(legend continued on next page)

Gli1^{NULL} SVZ, we quantified the rate of EdU incorporation in vNSCs overexpressing *Gli2* (Roessler et al., 2005) and in cells treated with GANT58 inhibitor to reduce *Gli2* expression *in vitro* (Lauth et al., 2007). GANT58 treatment did not change the proportion of *Gli1* fate-mapped vNSCs derived from the *Gli1*^{HET} or *Gli1*^{NULL} SVZ (Figure S2C) but reduced the *Gli2* mRNA expression by ~50% in the NSCs, comparable with that in *Gli2* heterozygous mice (data not shown). Conversely, overexpression of *Gli2* increased its expression about 2-fold in NSCs (data not shown) without affecting the proportion of *Gli1* fate-mapped cells (Figure S2C). Overexpression or inhibition of *Gli2* in the *Gli1*^{HET} vNSCs did not alter EdU incorporation (Figures 2F and 2G). However, decreasing *Gli2* in *Gli1*^{NULL} vNSCs increased EdU incorporation (0.6% ± 0.1% cells in control versus 9.9% ± 1.8% cells with GANT58 treatment) in fate-mapped vNSCs, while overexpression of *Gli2* had no effect (Figures 2F and 2G), indicating that inhibition of *Gli2* in combination with loss of *Gli1* increases the proliferation of vNSCs *in vitro*. The unchanged proliferation rate in *Gli1*^{NULL} vNSCs with *Gli2* overexpression is consistent with the lack of alteration in number of activated NSCs in *Gli1*^{NULL} vNSCs at peak demyelination. Thus, the decrease in recruitment of *Gli1* fate-mapped cells to the CC following demyelination on combined loss of *Gli1* and *Gli2* may not be due to a reduction in proliferation of vNSCs.

Taken together, these results indicate that *Gli2* is essential for recruitment of *Gli1*^{NULL} vNSC-derived cells to the site of demyelinating injury but does not affect their quiescence or activation following demyelination.

Combined Loss of *Gli1* and *Gli2* Increases Migration of vNSC-Derived Cells to the Olfactory Bulb on Demyelination

Our results raise the possibility that loss of *Gli2* could alter the physiological migration of vNSCs into the OB via the rostral migratory stream (RMS) in the demyelinated brain. Loss of *Gli2* in the healthy SVZ does not affect the deeper layer granule interneurons in the OB produced by vNSCs, suggesting that GLI2 is not essential for vNSC migration to the OB (Ihrie et al., 2011; Petrova et al., 2013; Young et al., 2007). However, the role of GLI2 in the migration of vNSCs-derived cells lacking GLI1 to the OB and upon demyelination is not clear. We quantified the number of fate-mapped *Gli1* cells in the OB of *Gli1*^{HET} and *Gli1*^{NULL} brains with varying levels of *Gli2* expression at 2 weeks of recovery from demyelination. Loss of *Gli1* did not alter the number of *Gli1* fate-mapped cells in the OB of healthy mice on regular diet (Figures 3A and 3B). However, following recovery from demyelination there was a significant increase in the number of fate-mapped *Gli1*^{NULL} vNSCs in the OB (2.6- ± 0.13-fold in *Gli1*^{NULL};*Gli2*^{HET} and 2.7- ± 0.41-fold in *Gli1*^{NULL};*Gli2*^{NULL}) compared with the *Gli1*^{HET} vNSCs (4,670 ± 1,040 cells/mm^3 in *Gli1*^{HET}; *Gli2*^{WT} versus 11,777 ± 1,898 cells/mm^3 in *Gli1*^{NULL}; *Gli2*^{HET} and 11,142 ± 1,168 cells/mm^3 in *Gli1*^{NULL}; *Gli2*^{NULL}) (Figures 3A and 3B). However, loss of *Gli2* did not affect the position and morphology of fate-mapped vNSCs within the OB following demyelination. Cells with neuronal morphology were located in the deeper granule cell layers and those with an astrocytic morphology were predominantly in the external plexiform layer of the OB (Figures 3A and 3A').

To determine the total number of vNSC-derived cells that had migrated out of the SVZ, we combined the fate-mapped cells recruited to the CC and the OB. Consistent with an increase in proliferation in *Gli1*^{NULL} SVZ on demyelination, we found a 2.16- ± 0.03-fold increase in the total *Gli1*^{NULL} NSC-derived cells compared with those from *Gli1*^{HET} NSCs (Figure 3C). This increase in total number of recruited cells in *Gli1*^{NULL} CC and OB remained constant irrespective of the *Gli2* gene dosage. In addition, loss of *Gli2* did not alter the percentage of *Gli1* fate-mapped vNSCs in the SVZ co-expressing the neuroblast marker doublecortin (DCX) at peak demyelination and at 2 weeks of recovery from demyelination, indicating that there was no reduction in generation of neuroblasts destined for the OB (Figures S3A–S3C). Since the total number of cells recruited out of the SVZ remained constant with loss of *Gli2* but the location of the recruited cells was altered with respect to the CC versus OB, these results also indicate that loss of *Gli2* redirects *Gli1*^{NULL} vNSC-derived cells from the site of demyelination to the RMS for migration to the OB. Together, these data show that, while inhibition of *Gli1* with simultaneous increase in *Gli2* promotes migration of vNSC-derived cells

(D) Immunofluorescence for co-expression of GFAP (magenta) and GFP (green) in fate-mapped *Gli1*^{HET} (left) or *Gli1*^{NULL} (right) vNSCs in the SVZ at 2 weeks of recovery from a cuprizone diet. Gli1 + GFAP + NSCs (arrows); Gli1 + GFAP- cells (arrowheads). Inset shows enlarged boxed area. n = 3 mice/genotype, Scale bars, 50 μm.

(E) Quantification of the proportion of fate-mapped *Gli1* vNSCs co-expressing GFAP (D) in *Gli1*^{HET} and *Gli1*^{NULL} mice. n = 3 mice/genotype.

(F) Immunofluorescence for EdU incorporation (green) in RFP + fate-mapped *Gli1* vNSCs (red) from *Gli1*^{HET} and *Gli1*^{NULL} mice *in vitro*. n = 3 replicates, Scale bar, 50 μm.

(G) Quantification of the proportion of RFP + fate-mapped *Gli1* vNSCs labeled by EdU in (F).

For (C), (E), and (G): one-way ANOVA within Gli1 groups followed by t tests comparing groups with controls. Data presented as mean ± SEM. CC, corpus callosum; SVZ, subventricular zone; CUP, cuprizone diet; REG, regular diet; Gli2-OE, Gli2 overexpression.

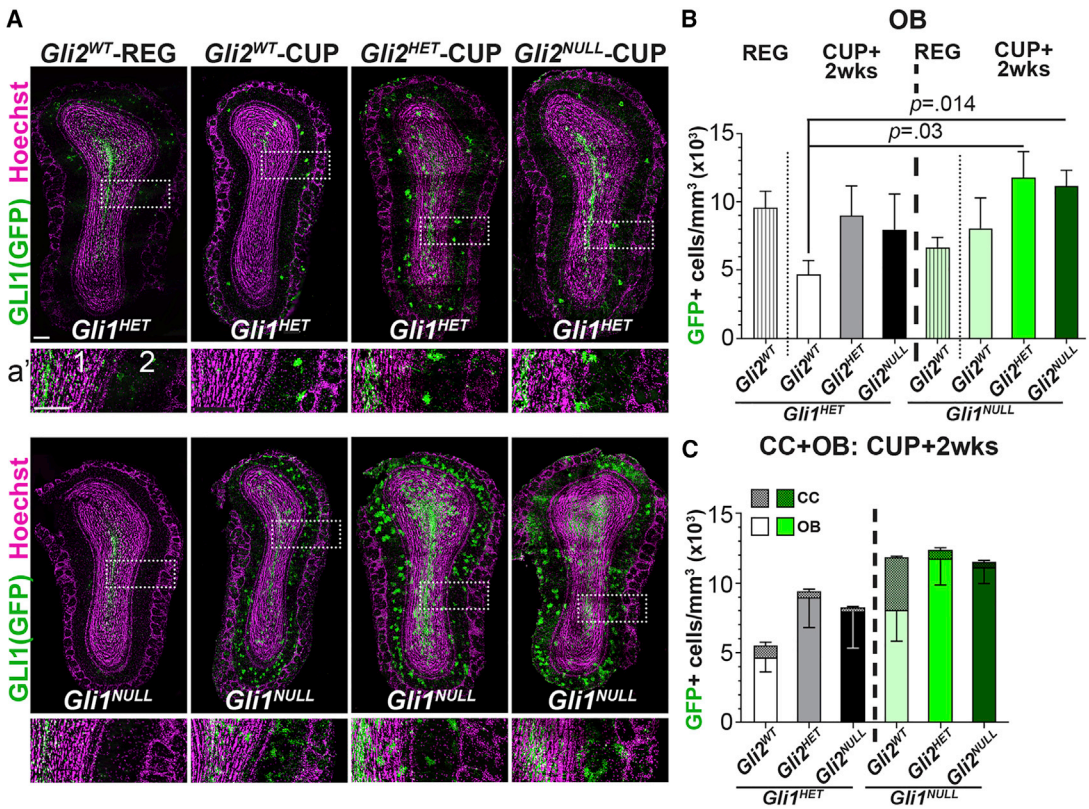

Figure 3. Ablation of *Gli2* Increases Recruitment of *Gli1*^{NULL} vNSC Progeny to the Olfactory Bulb

(A) Immunofluorescence for GFP + fate-mapped vNSCs (green) in *Gli1*^{HET} (top) and *Gli1*^{NULL} (bottom) OB on regular diet or at 2 weeks of recovery from a cuprizone diet. (A') Enlarged portion of the OB (dotted rectangle) showing (1) granule and (2) external plexiform layers.

(B) Quantification of the fate-mapped *Gli1*^{HET} and *Gli1*^{NULL} vNSCs in (A). One-way ANOVAs followed by multiple t tests within *Gli1* groups and comparing all groups with *Gli1*^{HET};*Gli2*^{WT} controls.

(C) Quantification of the combined number of fate-mapped *Gli1*^{HET} and *Gli1*^{NULL} cells in the CC and OB. One-way ANOVAs followed by multiple t tests within Gli1 groups.

Data presented as mean ± SEM; n = 3 mice/genotype. Scale bar, 50 μm. OB, olfactory bulb; CC, corpus callosum; SVZ, subventricular zone; CUP, cuprizone diet; REG, regular diet.

to demyelinated lesions, loss of both *Gli1* and *Gli2* prevents their recruitment toward the demyelinated lesion.

Gli2 Promotes the Differentiation of *Gli1*-null vNSC-Derived Cells into OLs

In the healthy brain, GLI2 is expressed in all NSCs in the SVZ and in parenchymal astrocytes, but not in cells of the OL lineage, including OPCs and mature OLs (Garcia et al., 2010). However, its role in cell fate decisions in the demyelinated brain remains unknown. We examined if loss of GLI2 altered the differentiation of the few vNSC-derived cells recruited to the CC in response to demyelination. Ablation of *Gli2* significantly reduced the number of fate-mapped mature OLs expressing CC1 in the *Gli1*^{NULL} callosum (81.2% ± 2.2% in *Gli1*^{NULL};*Gli2*^{WT} versus 24.9% ± 11.2% in *Gli1*^{NULL};*Gli2*^{HET} and 33.2% ± 12.3% in *Gli1*^{NULL};*Gli2*^{NULL}) but did not change the OLs in the *Gli1*^{HET} callosum at 2 weeks of recovery from a cuprizone diet (Figures 4A and 4B). Interestingly, loss of *Gli2* did not alter the generation of PDGFRα-expressing OPCs in the *Gli1*^{HET} and *Gli1*^{NULL} CC (Figures 4A and 4B) suggesting that GLI2 is required for terminal differentiation of OLs in the absence of GLI1. To further examine the effect of GLI2 on differentiation, we overexpressed and pharmacologically inhibited *Gli2* in the *Gli1* fate-mapped vNSCs from adult *Gli1*^{HET} and *Gli1*^{NULL} SVZ *in vitro*. Neither overexpression nor inhibition of *Gli2* expression in *Gli1*^{HET}- or *Gli1*^{NULL}-derived vNSCs changed the number of *Gli1* fate-mapped OPCs expressing NG2 (Figures 4C and 4D). However, overexpression of *Gli2* significantly increased the differentiation of *Gli1*^{NULL} vNSCs into mature OLs expressing MBP and this effect was abrogated by inhibition of *Gli2* (0.05% ± 0.03% in control cells versus 1.52% ± 0.35% on *Gli2* overexpression versus 0.03% ± 0.03% with GANT58 treatment)

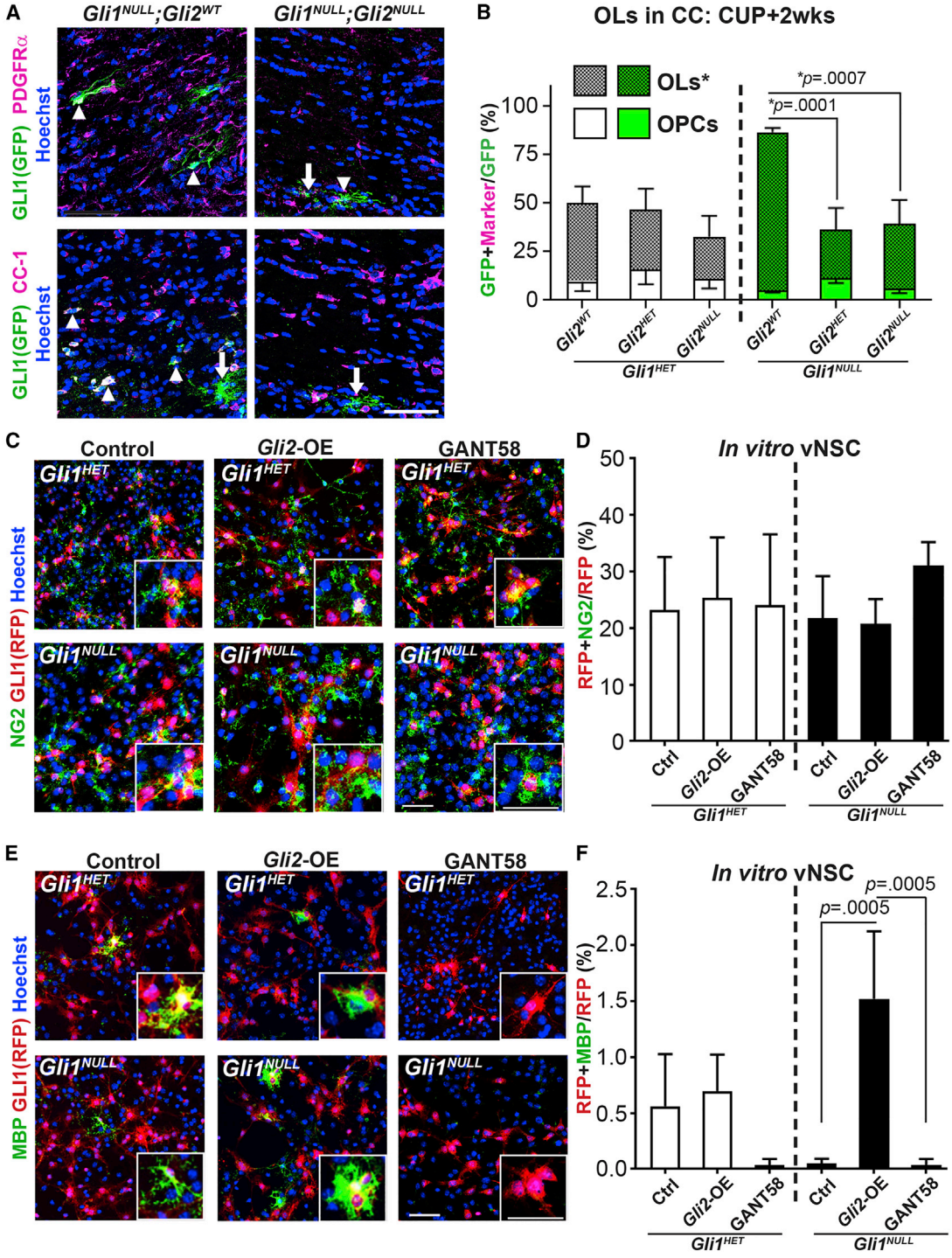

Figure 4. *Gli2* Promotes Oligodendrocyte Differentiation from vNSCs

(A) Immunofluorescence for fate-mapped *Gli1*^{NULL} vNSCs (green) co-expressing PDGFRα (OPC) or CC1 (OL) (magenta). n = 5 mice/genotype, GFP + cell (arrows) and marker + GFP co-expressing cells (arrowheads).

(B) Quantification of the proportion of GFP + fate-mapped *Gli1*^{HET} (white) and *Gli1*^{NULL} (green) vNSCs that co-express markers of OPC (PDGFRα) and OL (CC1) in (B).

(C) Immunofluorescence for OPCs (NG2, green) and RFP + *Gli1* fate-mapped vNSCs (red) following overexpression (Gli2-OE) or inhibition (GANT58 treatment) of *Gli2 in vitro*. n = 3 replicates.

(legend continued on next page)

(Figures 4E and 4F). These results indicate that overexpression of *Gli2* is necessary, in the absence of *Gli1*, for terminal differentiation to mature OLs.

To examine the role of GLI2 in astrocyte generation from vNSCs, we quantified the number of GFAP-expressing astrocytes and Nestin-expressing astrocytes/progenitor cells in the white matter following 2 weeks of recovery from a cuprizone diet *in vivo*. Interestingly, loss of *Gli2* reduced the proportion of *Gli1* fate-mapped cells expressing GFAP modestly in the $Gli1^{HET}$ CC (15.5% ± 2.4% in $Gli1^{HET}$;$Gli2^{WT}$ versus 0.4% ± 0.4% in $Gli1^{HET}$;$Gli2^{HET}$ and 1.7% ± 1.0% in $Gli1^{HET}$;$Gli2^{NULL}$), but had no effect on number of NESTIN-expressing cells (Figures S4A–S4C). However, the proportion of *Gli1* fate-mapped cells co-expressing GFAP and NESTIN were unaltered in the $Gli1^{NULL}$ CC irrespective of the *Gli2* gene dosage (Figures S4A–S4C). We further examined this effect on astrocyte differentiation *in vitro*, but did not detect any effect with overexpression or inhibition of *Gli2* in $Gli1^{HET}$- or $Gli1^{NULL}$-derived vNSCs (Figures S4D and S4E), suggesting that the *in vivo* effect on number of GFAP-expressing cells in $Gli1^{HET}$ CC is probably not a direct effect of loss of *Gli2*. Taken together, these results indicate that GLI2 is required for generation of mature OLs in the absence of GLI1, further highlighting the importance of relative expression levels of the two transcription factors following demyelination.

DISCUSSION

This study shows that GLI2 plays an essential role in differentiation and recruitment of vNSC-derived cells to demyelinated lesions in the absence of GLI1. We observed an increase in GLI2 expression following demyelination in the SVZ and when we ablated *Gli2* in the *Gli1*-deficient vNSCs, the resulting progeny were preferentially recruited to the OB. This altered recruitment pattern suggests that GLI2 expression may normally be required to divert $Gli1^{NULL}$ vNSC-derived cells toward the lesion. In addition, any cell that is recruited to the lesion may fail to differentiate into mature OLs in the absence of GLI2.

Gli1 knockout mice are viable and loss of GLI1 does not seem to alter the expression of Shh target genes (Lipinski et al., 2006). On the contrary, *Gli2* knockout mice as well as *Gli1/Gli2* double homozygous mutant mice show embryonic lethality (Bai et al., 2002; Park et al., 2000). Notably, global loss of *Gli1* combined with heterozygous ablation of *Gli2* also results in death soon after birth, indicating a haploinsufficient effect of *Gli2* (Park et al., 2000). While $Gli2^{HET}$ mice are considered normal, they show developmental defects following teratogen exposure, further underscoring the functional effects of *Gli2* haploinsufficiency (Heyne et al., 2016; Kietzman et al., 2014). *Gli2* has also been shown to promote migration of cranial neural crest and glioma cells in the brain (Huang et al., 2018; Timberlake et al., 2019). Similarly, our results showing reduction of recruitment of vNSC-derived cells to the demyelinated CC in $Gli1^{NULL}$; $Gli2^{HET}$ mice point to the role of *Gli2* haploinsufficiency.

Our data further show that overexpression of GLI2 is sufficient to increase differentiation into mature OLs by $Gli1^{NULL}$ but not by $Gli1^{HET}$ vNSCs, further indicating the distinct functions of relative levels of GLI1 and GLI2. This is consistent with studies showing different genes being activated by GLI1 alone or GLI2 alone or combined actions of both transcription factors (Tolosa et al., 2020). Although ablation of *Gli2* reduced astrocyte differentiation from $Gli1^{HET}$ vNSCs progeny recruited to the demyelinated CC, *in vitro* overexpression and inhibition of *Gli2* in these vNSCs did not alter their differentiation into astrocytes. In addition, loss of *Gli2* in $Gli1^{NULL}$ vNSCs did not alter astrocyte differentiation upon demyelination, similar to that observed in healthy brains where the loss of both GLI1 and GLI2 activity produces an activated phenotype without a change in the number of astrocytes (Garcia et al., 2010). These results suggest that GLI2 does not play a direct role in astrocyte differentiation. Alternatively, these data may reflect differences in the microenvironment upon demyelination. Indeed, demyelination changes the expression of several growth factors, including fibroblast growth factor and transforming growth factor β1 (Huang and Dreyfus, 2016), which can regulate *Gli2* expression (Brewster et al., 2000; Javelaud et al., 2011) and astrocyte generation (Nataf, 2020; Savchenko et al., 2019).

Taken together, our results indicate that GLI2 is necessary in the absence of GLI1 for enhanced migration of vNSC progeny and oligodendrogenesis in demyelinated lesions. These data highlight that GLI1 and GLI2 have distinct functions in response to demyelination, consistent with their distinct transcriptional targets (Ali et al., 2019; Tolosa et al., 2020). They also suggest that therapeutic strategies that target the

(D) Quantification of *Gli2* overexpression or inhibition in (C).
(E) Immunofluorescence for MBP + mature OLs (green) and RFP + fate-mapped *Gli1* vNSCs (red) following overexpression (Gli2-OE) or inhibition (GANT58 treatment) of *Gli2 in vitro*. n = 3 replicates.
(F) Quantification of *Gli2* overexpression (Gli2-OE) or inhibition (GANT58 treatment) in (E).
One-way ANOVA with Tukey's post-hoc t tests within Gli1 genotypes; all data presented as mean ± SEM. Scale bars, 50 μm. CC, corpus callosum; OPC, oligodendrocyte progenitor cells; OL, oligodendrocyte; CUP, cuprizone diet; Gli2-OE, *Gli2*-overexpression.

transcriptional effectors of Shh (Lauth et al., 2007) could have very different outcomes depending on the relative specificity for GLI1 versus GLI2. In conclusion, our results indicate that specific GLI1 inhibitors that do not target GLI2 may be required for enhancing remyelination.

EXPERIMENTAL PROCEDURES

Fate Mapping and Demyelination

All animals were maintained according to the SVM IACUC protocols at University of Wisconsin-Madison. Mouse lines obtained from Jackson Laboratory: *Gli1*^{CreERT2} (Jax no. 007913), *Gli1*^{nLacZ} (Jax no. 008211), *Gli2*^{Flox} (Jax no. 007926), *Rosa-CAG-EGFP* (*RCE*) (Jax no. 032037) for *in vivo* experiments and *Rosa-CAG-TdTomato* (*Ai9*) (Jax no. 007909) for *in vitro* experiments. The genotypes used: *Gli1*^{HET};*Gli2*^{WT} (*Gli1*$^{CreER/WT}$;*RCE*$^{FX/FX}$), *Gli1*^{HET};*Gli2*^{HET} (*Gli1*$^{CreER/WT}$;*Gli2*$^{FX/WT}$;*RCE*$^{FX/FX}$), *Gli1*^{HET};*Gli2*^{NULL} (*Gli1*$^{CreER/WT}$;*Gli2*$^{FX/FX}$;*RCE*$^{FX/FX}$), *Gli1*^{NULL};*Gli2*^{WT} (*Gli1*$^{CreER/CreER}$;*RCE*$^{FX/FX}$), *Gli1*^{NULL};*Gli2*^{HET} (*Gli1*$^{CreER/CreER}$;*Gli2*$^{FX/WT}$;*RCE*$^{FX/FX}$), and *Gli1*^{NULL};*Gli2*^{NULL} (*Gli1*$^{CreER/CreER}$;*Gli2*$^{FX/FX}$;*RCE*$^{FX/FX}$) for *in vivo* analysis; and for *in vitro* analysis: *Gli1*^{HET} (*Gli1*$^{CreER/WT}$;*Ai9*$^{FX/WT}$) and *Gli1*^{NULL} (*Gli1*$^{CreERT2/CreERT2}$;*Ai9*$^{FX/WT}$). All mice were maintained on C57Bl/6 background. For fate mapping, 10-week-old mice were administered 5 mg/day tamoxifen (no. 13258, Cayman Chemical, Ann Arbor, MI) in corn oil for four intraperitoneal injections on alternate days. No labeling was seen in the absence of tamoxifen administration. Demyelination was induced 1 week after tamoxifen administration by feeding 0.2% cuprizone in the chow for 5–6 weeks.

In Vivo Immunofluorescence

Cryosections were processed for immunofluorescence with rabbit or chicken anti-GFP antibody and these antibodies: rat anti-PDGFRα; mouse anti-CC1, anti-GFAP, anti-MBP, and anti-LacZ, guinea pig anti-GLI2 (1:50, kind gift from Jonathan Eggenschwiler, University of Georgia) (Cho et al., 2008), and anti-donkey or anti-goat secondary antibodies conjugated with Alexa Fluor (Table S1). Nuclei were counterstained with Hoechst 33258 (1:5,000, Invitrogen, no. H3570).

Primary NSC Culture

Seven- to 12-week-old *Gli1*$^{CreER/WT}$;*Ai9*$^{FX/WT}$ or *Gli1*$^{CreER/CreER}$;*Ai9*$^{FX/WT}$ mice were administered 5 mg of tamoxifen to fate-map *Gli1*-expressing cells 3 days before euthanasia. The SVZ from two brains were pooled for each NSC culture as described in the Supplemental Experimental Procedures .

In Vitro Immunofluorescence

NSCs plated on Matrigel-coated coverslips were fixed in ice-cold methanol and labeled with the primary antibodies, including: rabbit anti-NG2 and rat anti-RFP to label TdTomato (Table S1). Images were analyzed as described in the Supplemental Experimental Procedures.

Statistical Analysis

All experiments were replicated at least three times. For *in vivo* experiments, at least five sections per mouse were analyzed and data from three to five mice were combined. All data are expressed as mean ± standard error of mean. Statistical analysis was performed using Student's t test, one-way ANOVA, or two-way ANOVA with Tukey's post-hoc t test. Differences were considered statistically significant at $p < 0.05$.

SUPPLEMENTAL INFORMATION

Supplemental Information can be found online at https://doi.org/10.1016/j.stemcr.2020.10.003.

AUTHOR CONTRIBUTIONS

D.Z.R., J.S., and H.M.M. performed the research, analyzed and interpreted the results, and edited the manuscript. S.K.B., E.D.C., M.M.T., and C.A.O. performed imaging and *in vitro* cell counts. J.R.H.-S. performed preliminary cell counts. J.S. designed the experiments and wrote the manuscript. J.L.S. edited the manuscript.

CONFLICTS OF INTERESTS

A patent on the method of targeting GLI1 as a strategy to promote remyelination has been awarded, with J. L.S., J.S., and G.F. listed as co-inventors. J.L.S. is a consultant for and has ownership interests in Glixogen Therapeutics.

ACKNOWLEDGMENTS

This research was supported by grants to J.L.S. from NIH NS0100867 and NY State DOH01-STEM5-2016-00305 and to J.S. from the Nancy and Jean-Pierre Boespflug Foundation for Myopathic Research.

Received: May 30, 2019
Revised: October 2, 2020
Accepted: October 2, 2020
Published: October 29, 2020

REFERENCES

Ahn, S., and Joyner, A.L. (2005). In vivo analysis of quiescent adult neural stem cells responding to Sonic hedgehog. Nature *437*, 894–897.

Ali, S.A., Niu, B., Cheah, K.S.E., and Alman, B. (2019). Unique and overlapping GLI1 and GLI2 transcriptional targets in neoplastic chondrocytes. PLoS One *14*, e0211333.

Bai, C.B., Auerbach, W., Lee, J.S., Stephen, D., and Joyner, A.L. (2002). Gli2, but not Gli1, is required for initial Shh signaling and ectopic activation of the Shh pathway. Development *129*, 4753–4761.

Brewster, R., Mullor, J.L., and Ruiz i Altaba, A. (2000). Gli2 functions in FGF signaling during antero-posterior patterning. Development *127*, 4395–4405.

Chaker, Z., Codega, P., and Doetsch, F. (2016). A mosaic world: puzzles revealed by adult neural stem cell heterogeneity. Wiley Interdiscip. Rev. Dev. Biol. *5*, 640–658.

Cho, A., Ko, H.W., and Eggenschwiler, J.T. (2008). FKBP8 cell-autonomously controls neural tube patterning through a Gli2- and Kif3a-dependent mechanism. Dev. Biol. *321*, 27–39.

Codega, P., Silva-Vargas, V., Paul, A., Maldonado-Soto, A.R., Deleo, A.M., Pastrana, E., and Doetsch, F. (2014). Prospective identification and purification of quiescent adult neural stem cells from their in vivo niche. Neuron *82*, 545–559.

Garcia, A.D., Petrova, R., Eng, L., and Joyner, A.L. (2010). Sonic hedgehog regulates discrete populations of astrocytes in the adult mouse forebrain. J. Neurosci. *30*, 13597–13608.

Heyne, G.W., Everson, J.L., Ansen-Wilson, L.J., Melberg, C.G., Fink, D.M., Parins, K.F., Doroodchi, P., Ulschmid, C.M., and Lipinski, R.J. (2016). Gli2 gene-environment interactions contribute to the etiological complexity of holoprosencephaly: evidence from a mouse model. Dis. Models Mech. *9*, 1307–1315.

Huang, D., Wang, Y., Xu, L., Chen, L., Cheng, M., Shi, W., Xiong, H., Zalli, D., and Luo, S. (2018). GLI2 promotes cell proliferation and migration through transcriptional activation of ARHGEF16 in human glioma cells. J. Exp. Clin. Cancer Res. *37*, 247.

Huang, Y., and Dreyfus, C.F. (2016). The role of growth factors as a therapeutic approach to demyelinating disease. Exp. Neurol. *283*, 531–540.

Ihrie, R.A., Shah, J.K., Harwell, C.C., Levine, J.H., Guinto, C.D., Lezameta, M., Kriegstein, A.R., and Alvarez-Buylla, A. (2011). Persistent sonic hedgehog signaling in adult brain determines neural stem cell positional identity. Neuron *71*, 250–262.

Javelaud, D., Alexaki, V.I., Dennler, S., Mohammad, K.S., Guise, T.A., and Mauviel, A. (2011). TGF-β/SMAD/GLI2 signaling axis in cancer progression and metastasis. Cancer Res. *71*, 5606–5610.

Kietzman, H.W., Everson, J.L., Sulik, K.K., and Lipinski, R.J. (2014). The teratogenic effects of prenatal ethanol exposure are exacerbated by Sonic Hedgehog or GLI2 haploinsufficiency in the mouse. PLoS One *9*, e89448.

Lauth, M., Bergstrom, A., Shimokawa, T., and Toftgard, R. (2007). Inhibition of GLI-mediated transcription and tumor cell growth by small-molecule antagonists. Proc. Natl. Acad. Sci. U S A *104*, 8455–8460.

Lipinski, R.J., Gipp, J.J., Zhang, J., Doles, J.D., and Bushman, W. (2006). Unique and complimentary activities of the Gli transcription factors in Hedgehog signaling. Exp. Cell Res. *312*, 1925–1938.

Matsushima, G.K., and Morell, P. (2001). The neurotoxicant, cuprizone, as a model to study demyelination and remyelination in the central nervous system. Brain Pathol. *11*, 107–116.

Mo, R., Freer, A.M., Zinyk, D.L., Crackower, M.A., Michaud, J., Heng, H.H., Chik, K.W., Shi, X.M., Tsui, L.C., Cheng, S.H., et al. (1997). Specific and redundant functions of Gli2 and Gli3 zinc finger genes in skeletal patterning and development. Development *124*, 113–123.

Nataf, S. (2020). The demonstration of an Aqp4/Tgf-beta 1 pathway in murine astrocytes holds implications for both neuromyelitis optica and progressive multiple sclerosis. Int. J. Mol. Sci. *21*. https://doi.org/10.3390/ijms21031035.

Park, H.L., Bai, C., Platt, K.A., Matise, M.P., Beeghly, A., Hui, C.C., Nakashima, M., and Joyner, A.L. (2000). Mouse Gli1 mutants are viable but have defects in SHH signaling in combination with a Gli2 mutation. Development *127*, 1593–1605.

Petrova, R., Garcia, A.D., and Joyner, A.L. (2013). Titration of GLI3 repressor activity by sonic hedgehog signaling is critical for maintaining multiple adult neural stem cell and astrocyte functions. J. Neurosci. *33*, 17490–17505.

Roessler, E., Ermilov, A.N., Grange, D.K., Wang, A., Grachtchouk, M., Dlugosz, A.A., and Muenke, M. (2005). A previously unidentified amino-terminal domain regulates transcriptional activity of wild-type and disease-associated human GLI2. Hum. Mol. Genet. *14*, 2181–2188.

Samanta, J., Grund, E.M., Silva, H.M., Lafaille, J.J., Fishell, G., and Salzer, J.L. (2015). Inhibition of Gli1 mobilizes endogenous neural stem cells for remyelination. Nature *526*, 448–452.

Sanchez, M.A., and Armstrong, R.C. (2018). Postnatal Sonic hedgehog (Shh) responsive cells give rise to oligodendrocyte lineage cells during myelination and in adulthood contribute to remyelination. Exp. Neurol. *299*, 122–136.

Savchenko, E., Teku, G.N., Boza-Serrano, A., Russ, K., Berns, M., Deierborg, T., Lamas, N.J., Wichterle, H., Rothstein, J., Henderson, C.E., et al. (2019). FGF family members differentially regulate maturation and proliferation of stem cell-derived astrocytes. Sci. Rep. *9*, 9610.

Timberlake, A.T., Jin, S.C., Nelson-Williams, C., Wu, R., Furey, C.G., Islam, B., Haider, S., Loring, E., Galm, A., Yale Center for Genome, A., et al. (2019). Mutations in TFAP2B and previously unimplicated genes of the BMP, Wnt, and Hedgehog pathways in syndromic craniosynostosis. Proc. Natl. Acad. Sci. U S A *116*, 15116–15121.

Tolosa, E.J., Fernandez-Barrena, M.G., Iguchi, E., McCleary-Wheeler, A.L., Carr, R.M., Almada, L.L., Flores, L.F., Vera, R.E., Alfonse, G.W., Marks, D.L., et al. (2020). GLI1/GLI2 functional interplay is required to control Hedgehog/GLI targets gene expression. Biochem. J. *477*, 3131–3145.

Young, K.M., Fogarty, M., Kessaris, N., and Richardson, W.D. (2007). Subventricular zone stem cells are heterogeneous with respect to their embryonic origins and neurogenic fates in the adult olfactory bulb. J. Neurosci. *27*, 8286–8296.

Stem Cell Reports, Volume *15*

Supplemental Information

Relative Levels of *Gli1* and *Gli2* Determine the Response of Ventral Neural Stem Cells to Demyelination

Daniel Z. Radecki, Heather M. Messling, James R. Haggerty-Skeans, Sai Krishna Bhamidipati, Elizabeth D. Clawson, Christian A. Overman, Madison M. Thatcher, James L. Salzer, and Jayshree Samanta

Relative levels of *Gli1* and *Gli2* determine the response of ventral Neural Stem Cells to demyelination

SUPPLEMENTAL FIGURES AND LEGENDS:

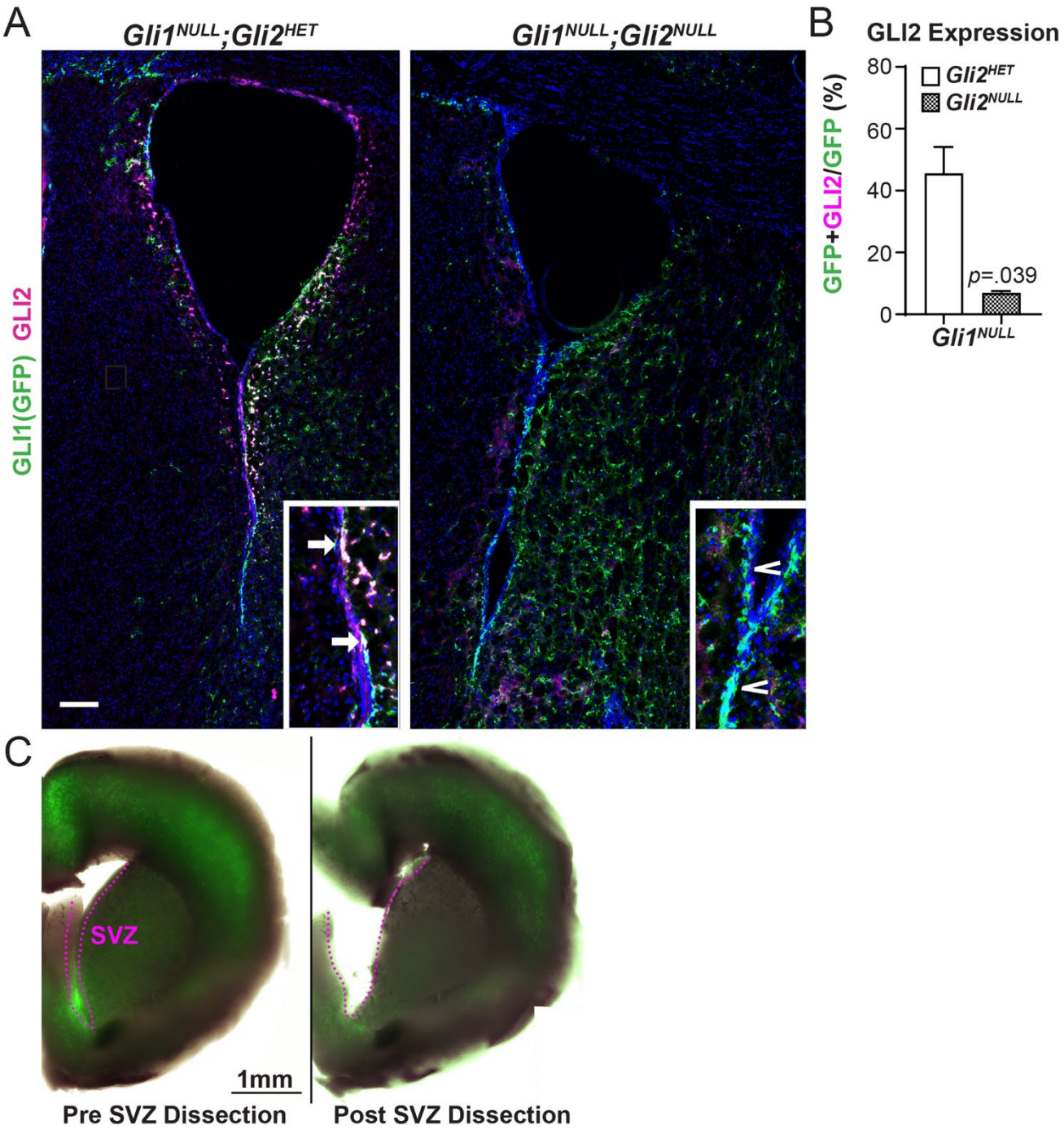

Figure S1 – Recombination efficiency of *Gli2* in GLI1 vNSCs and SVZ dissection (Related to Figure 2 and Methods).

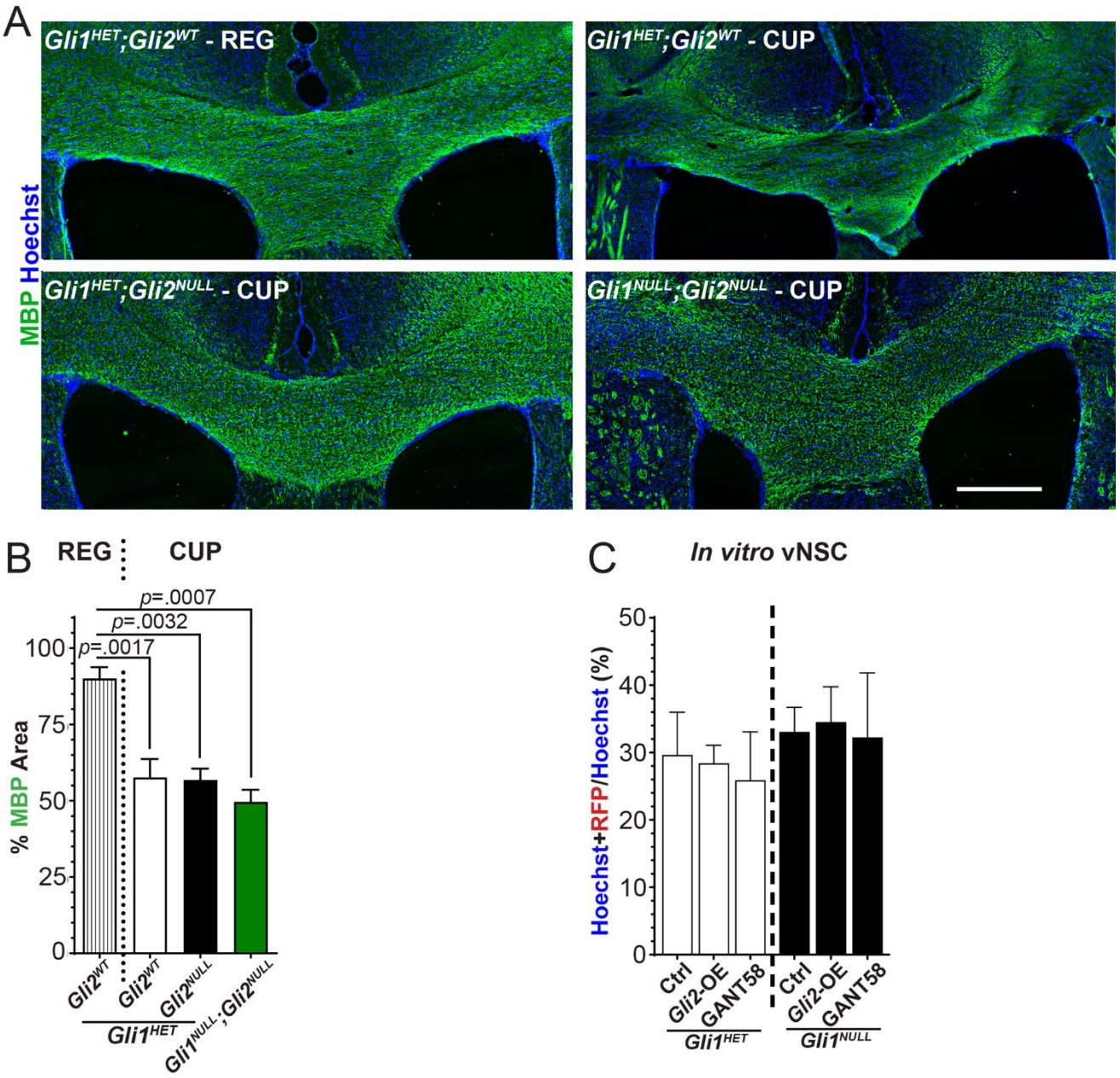

Figure S2 – Demyelination extent in the CC with *in vitro* mRNA and fate-mapping analysis. (Related to Figure 2).

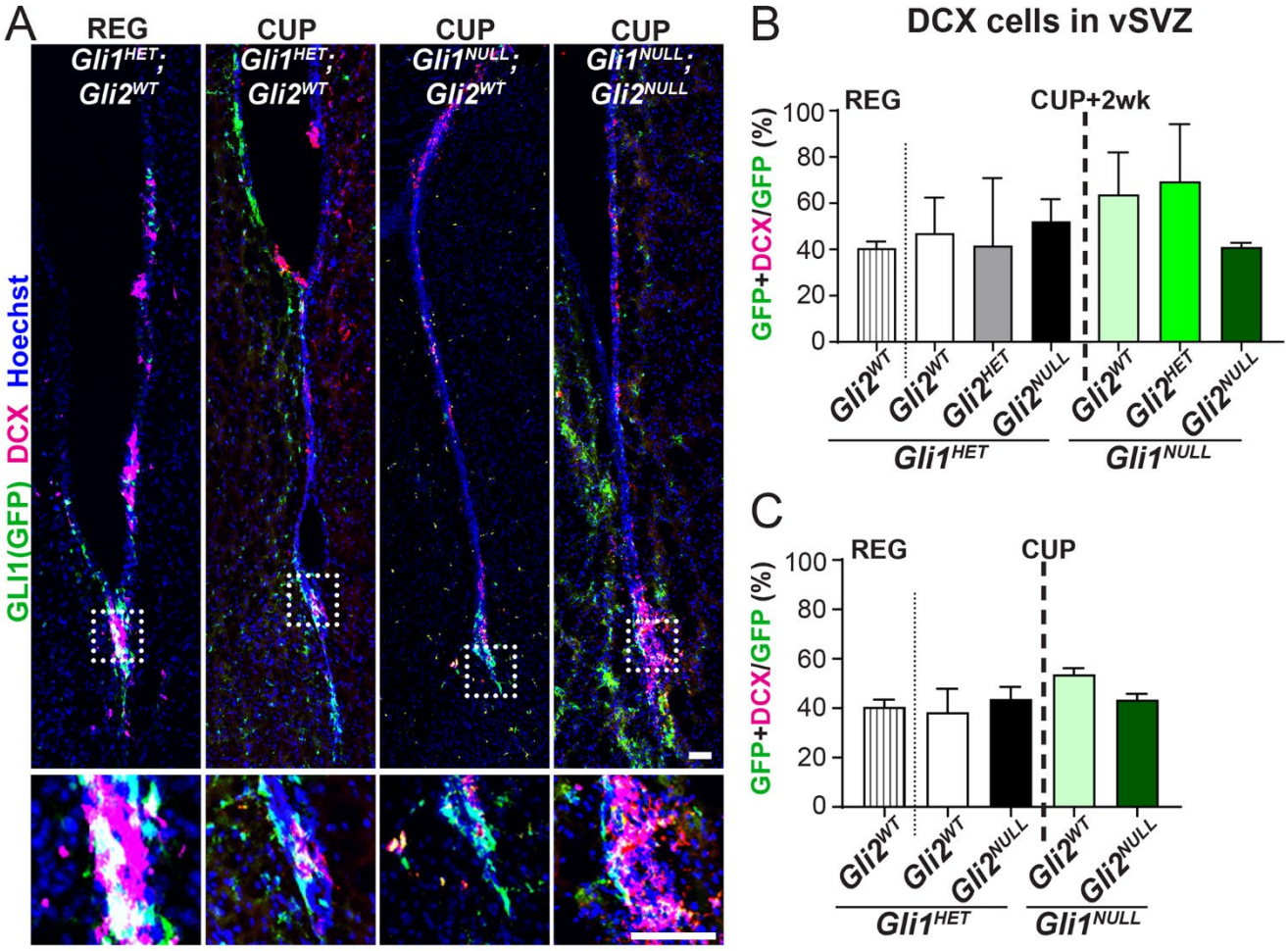

Figure S3 – Differentiation of GLI1 vNSCs into neuroblasts in the SVZ following demyelination (Related to Figure 3).

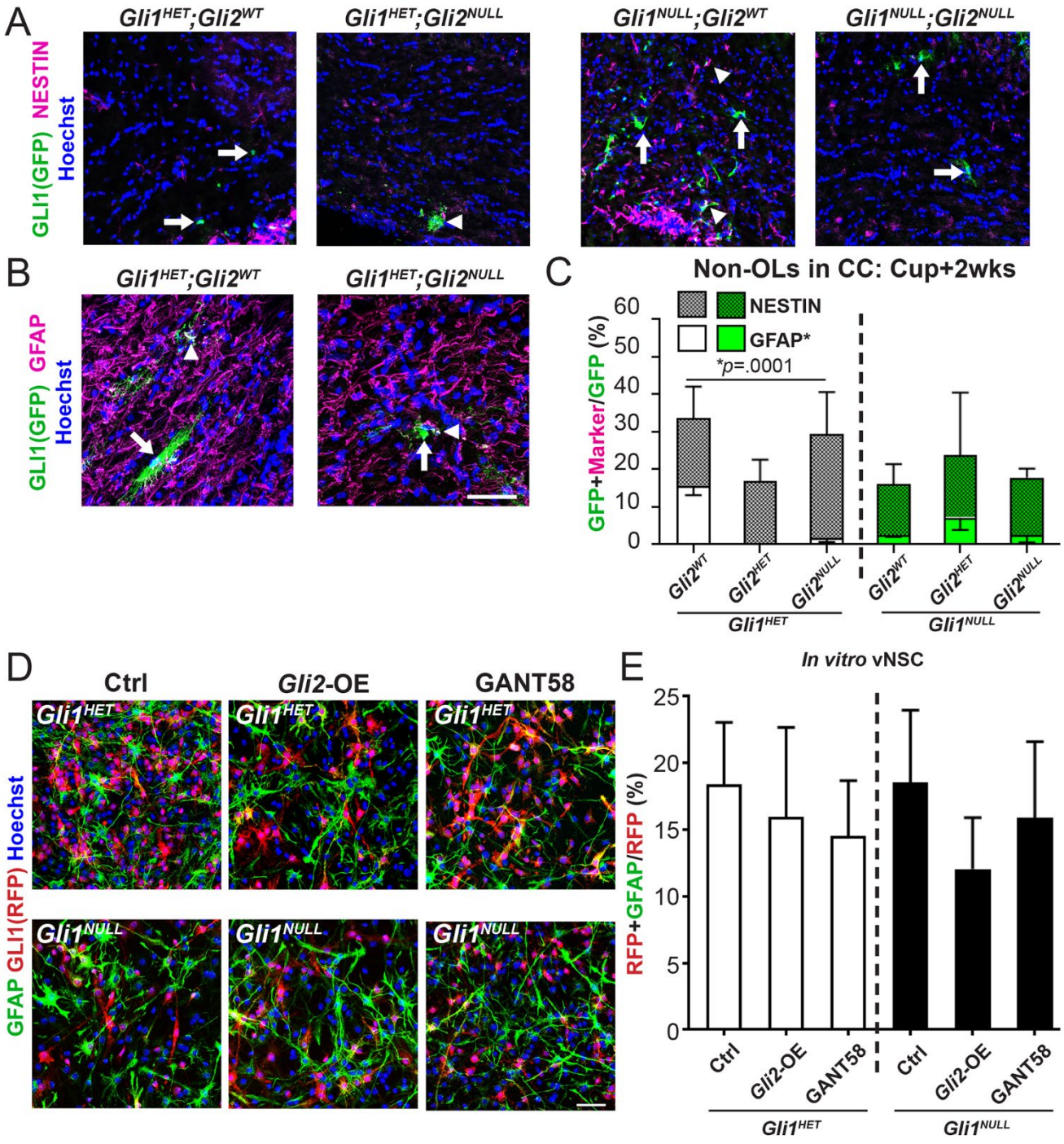

Figure S4 – Astrocyte differentiation from vNSCs (Related to Figure 4).

Figure S1 – Recombination efficiency of *Gli2* in *Gli1* vNSCs and SVZ dissection (Related to Figure 2 and Methods).

A) Immunofluorescence for GFP+ *Gli1* fate-mapped cells (green) and GLI2 expression (magenta) in the subventricular zone (SVZ) showing GFP+GLI2+ cells (left inset, arrows) in $Gli2^{HET}$ vNSCs and GFP+GLI2- cells (right inset, arrowheads) in $Gli2^{NULL}$ vNSCs. Scale bar=250µm.

B) Quantification of (A) shows a reduction in the percentage of *Gli1* vNSCs expressing GLI2 in the $Gli2^{NULL}$ SVZ. Unpaired t-test comparing $Gli2^{HET}$ and $Gli2^{NULL}$ animals; all data presented as mean ± SEM; n=3 mice/genotype.

C) Fluorescent image overlaid on brightfield image of a slice from *Gli1* (GFP, green) fate-mapped mouse before dissecting the SVZ (left) and after removal of the SVZ (right)(magenta outline).

Figure S2 – Demyelination extent in the CC with *in vitro* mRNA and fate-mapping analysis. (Related to Figure 2).

A) Immunofluorescence for MBP+ myelin in the CC of mice on regular diet or cuprizone diet.

B) Quantification of the MBP+ area throughout the CC in (A) showed a significant decrease at 5wks of cuprizone diet.

C) Quantification of the number of RFP+ *Gli1* fate-mapped vNSCs *in vitro* showed no change on overexpression or inhibition of *Gli2*.

All tests are 1-way ANOVAs with Tukey's post-hoc t-tests. Data presented as mean ± SEM, n=3; scale = 200µm. Regular Diet (REG), Cuprizone diet (CUP), Ventral neural stem cells (vNSCs), *Gli2*-overexpression (Gli2-OE).

Figure S3 – Differentiation of *Gli1* vNSCs into neuroblasts in the SVZ following demyelination (Related to Figure 3).

A) Immunofluorescence for DCX+ neuroblasts (magenta) and GFP+ fate-mapped *Gli1* vNSCs (green) in the SVZ of mice on regular diet or at 2wks of recovery from cuprizone diet.

B) Quantification of the number of GFP+DCX+ cells in the SVZ at 2wks of recovery from cuprizone diet in (A).

C) Quantification of the number of GFP+DCX+ cells in the SVZ at peak demyelination (5wks of cuprizone diet).

One-way ANOVA with post-hoc t-tests; data presented as mean ± SEM; n=3, scale=25µm. Regular Diet (REG), Cuprizone diet (CUP), Ventral sub-ventricular zone (vSVZ).

Figure S4 – Astrocyte differentiation from vNSCs (Related to Figure 4).

A) Immunofluorescence for GFP+ fate-mapped vNSCs (green) in $Gli1^{HET}$ and $Gli1^{NULL}$ CC co-expressing the progenitor marker NESTIN (magenta). n= 3 mice/genotype

B) Immunofluorescence for GFP+ fate-mapped $Gli1^{HET}$ vNSCs (green) and the astrocytic marker GFAP (magenta). n= 3 mice/genotype.

C) Quantification of the proportion of GFP+ fate-mapped $Gli1^{HET}$ (white) and $Gli1^{NULL}$ (green) vNSCs co-expressing NESTIN (A) and GFAP (B) shows a decrease in astrocytes in the $Gli1^{HET}$ CC with loss of one or both copies of *Gli2*. n= 3 mice/genotype

D) Immunofluorescence for RFP+ fate-mapped vNSCs (red) from $Gli1^{HET}$ and $Gli1^{NULL}$ SVZ co-expressing the astrocytic marker GFAP (green) after 7 days of differentiation *in vitro*.

E) Quantification of RFP+GFAP+ cells in (D) shows no difference with *Gli2*-overexpression (Gli2-OE) or inhibition with GANT58. n=3 replicates

1-way ANOVAs with Tukey's post-hoc t-tests; all data presented as mean ± SEM; Scale bars=50µm. Ventral neural stem cells (vNSCs), corpus callosum (CC), Cuprizone diet (CUP), *Gli2*-overexpression (Gli2-OE).

EXPERIMENTAL PROCEDURES

In vivo **Immunofluorescent image analysis:** Mice were perfused with 4% PFA and coronal sections were acquired starting from the olfactory bulb rostrally to the anterior hippocampus caudally. For each analysis, we used 10 sections through the corpus callosum, each section was 20um thick with 200um distance between 2 sections, thus sampling the entire rostrocaudal span of the corpus callosum. Epifluorescent images were obtained as Z-stacks of 5µm optical sections using a Keyence BZ-X700 microscope with inbuilt automatic deconvolution at 20x magnification. For quantification of CC1, PDGFRα, GFAP, MBP and OB GFP immunostaining, the Keyence BZ-X Analyzer Hybrid Cell Count tool was used to count cells that were positive for Hoechst nuclei and the antibody labeled cells. A threshold was determined for each antibody and CNS location, then images were cropped to include either the cingulum of the CC, a 30□m section around the SVZ, or the entire olfactory bulb. Images from all animals were batch counted to avoid biases in manual cell counting, and results were collated in Microsoft Excel before analysis in GraphPad Prism. We also acquired z-stack images with the Leica confocal microscope to confirm the co-expression of different markers and manually counted a subset of images in ImageJ. We did not detect a difference between the manual and automatic cell counts. Publication quality images were obtained as Z-stacks of 1µm optical sections using a confocal laser-scanning microscope (Leica TCS SP8) and processed using Adobe Photoshop. The investigators were blinded to allocation during experiments and outcome assessment.

Primary NSC culture: The brains were harvested from mice after euthanasia and placed in an acrylic mouse brain mold (BS-A-5000C - Braintree Scientific) and 1mm slices were acquired from the caudal aspect of the olfactory bulbs to the dorsal hippocampus. Brain slices were moved to dissection media composed of DMEM/F-12 (#11320033 – Gibco) with 1x Antibiotic-Antimycotic (#15240112 – Gibco) and the SVZ tissue lining the ventral and lateral aspects of the lateral ventricles was microdissected from 3 consecutive slices (Fig. S1C). The dissected SVZ tissue was minced and collected by centrifugation for 5min x 400g. The tissue was then digested with 0.05% Trypsin-EDTA (#25300062, Gibco) and incubated at 37˚C for 5min with agitation every 60-90secs to form a cell suspension. After neutralizing the Trypsin-EDTA with 1mg/mL Soybean Trypsin Inhibitor (#17075029, Gibco), the cells were needle triturated and resuspended in Mouse NSC Proliferation Media (1x Anti-Anti, 10ng/mL bFGF (#78003, Stem Cell Tech, Vancouver), 20ng/mL mEGF (#78016 Stem Cell Tech), 0.0002% Heparin Sulfate (#H7640, Sigma), 1x Mouse Proliferation Supplement in NeuroCult Media (#5702 Stem Cell Tech Kit). The dissociated cells were then grown as floating neurospheres in proliferation media at 37˚C and 5% CO_2. Primary NSCs were supplemented with fresh bFGF and mEGF at day 3 and day 5 after plating. Neurospheres were passaged at day 7 to generate secondary neurospheres. Secondary neurospheres were dissociated into single cells and plated on Matrigel (#356234 Corning, concentration tested by WiCell) coated coverslips in differentiation media (1x Anti-Anti, 1ng/mL bFGF, 2ng/mL mEGF, 0.0002% Heparin, 1x Differentiation Supplement in Neurocult Media (#5704 Stem Cell Tech Kit). Cells were maintained in Differentiation Media for 7 days with half media changes every other day, then harvested for RNA or fixed in ice-cold methanol for 15min for immunolabelling.

In vitro **Immunofluorescent image analysis:** Images were acquired using Keyence BZ-X700 epifluorescent microscope from 10 fields per coverslip, for total 3 coverslips per marker per experimental group. Each experiment was repeated 3 times and the cell counts were averaged together. Total RFP+ (fate-mapped) cells were counted using Keyence software, while NG2+ (OPCs), MBP+ (OLs), and GFAP+ (Astrocytes) cells were counted manually using ImageJ.

qRT-PCR: SVZ was dissected (Fig. S1C) by slicing the brains into 1mm coronal sections and cutting the SVZ from each slice using 1mm spring scissors under a dissecting microscope. The SVZ was defined as the CNS tissue between the lateral ventricles and striatum (identified by white matter bundles) in the 3mm, 4mm, and 5mm slices caudal to the olfactory bulb. mRNA was extracted from three mice per genotype using RNeasy kit (Qiagen) and reverse-transcribed to complementary DNA using iScript cDNA Synthesis Kit (BioRad). ITaq Universal SYBR Green Supermix (BioRad) was used to perform qPCRs in a Biorad CFX Connect thermal cycler. Primers used were Gli2 (forward, 5'-AGA GAC AGC AGA AGC TAT GCC CAA-3'; reverse, 5'-TGG GCA GCC TCC ATT CTG TTC ATA-3') and GAPDH (forward, 5'-GGT GTG AAC GGA TTT GGC CGT ATT G-3'; reverse, 5'-CCG TTG AAT TTG CCG TGA GTG GAG T-3'). The $2^{-\Delta\Delta Ct}$ method was used to analyze the relative gene expression, each Gli1 genotype was normalized to regular diet.

GANT58 Treatment: GANT58 (#14193, Cayman Chemicals) was dissolved in DMSO at a concentration of 50mM and added to differentiating vNSCs beginning 2-3hrs after plating at a final concentration of 50uM. Fresh GANT58 was added every other day coinciding with media changes. An equal volume of DMSO was added to cells as a control.

Gli2 **overexpression:** $2x10^6$ dissociated NSCs were Nucleofected with the *pCS2-MT GLI2 FL* plasmid (a gift from Erich Roessler, Addgene plasmid # 17648) using the Lonza Mouse Neural Stem Cell Nucleofector Kit (#VPG-1004, Lonza) with Amaxa Nucleofector II.

EdU labeling: On day 7 of NSC differentiation, 10mM 5-ethynyl-2'-deoxyuridine (EdU) (#20518 Cayman Chemicals, MI) was dissolved in DMSO and added to cells in differentiation media at a final concentration of 10uM for 1hr before fixation. EdU was detected with the Click-IT EdU Kit – Alexa 647 (#C10340 Invitrogen) following the manufacturer's instructions.

Table S1: Antibodies used for immunofluorescence

Antibody	Concentration	Company	Catalog number
Rabbit anti-GFP	1:1000	Thermo Fisher Scientific	A-11122
Chicken anti-GFP	1:1000	Thermo Fisher Scientific	A-10262
rat anti-PDGFRα	1:200	BD Biosciences	562171
Mouse anti-CC1	1:400	Millipore	OP-80
Mouse anti-GFAP (GA-5)	1:400	Novus Biologicals	NBP2-29415
Rabbit anti-GFAP	1:400	Thermo Fisher Scientific	PA1-10019
Mouse anti-MBP	1:500	Biolegend	808402
Mouse anti-LacZ	1:2000	Sigma Aldrich	G8021
Rabbit anti-NG2	1:200	Millipore	AB5320
Rat anti-RFP	1:1000	Chromatek	5f8
Goat anti-Mouse Alexa 488 secondary Ab	1:1000	Thermo Fisher Scientific	A32723
Goat anti-Mouse Alexa 568 secondary Ab	1:1000	Thermo Fisher Scientific	A11004
Goat anti-Mouse Alexa 488 secondary Ab	1:1000	Thermo Fisher Scientific	A11008
Goat anti-Rabbit Alexa 568 secondary Ab	1:1000	Thermo Fisher Scientific	A11036
Goat anti-Guinea Pig Alexa 488 secondary Ab	1:1000	Thermo Fisher Scientific	A11073
Goat anti-Chicken Alexa 488 secondary Ab	1:1000	Thermo Fisher Scientific	A32932
Goat anti-Rat Alexa 488 secondary Ab	1:1000	Thermo Fisher Scientific	A11006
Goat anti-Rat Alexa 568 secondary Ab	1:1000	Thermo Fisher Scientific	A11077